Theory of FID NMR Signal Dephasing Induced by Mesoscopic Magnetic Field Inhomogeneities in Biological Systems

Alexander L. Sukstanskii and Dmitriy A. Yablonskiy

Mallinckrodt Institute of Radiology, Washington University School of Medicine, Campus Box 8227, 4525 Scott Avenue, St. Louis, Missouri 63110

E-mail: yablonskiyd@mir.wustl.edu

A theory of the NMR signal dephasing due to the presence of tissue-specific magnetic field inhomogeneities is developed for a two-compartment model. Randomly distributed magnetized objects of finite size embedded in a given media are modeled by ellipsoids of revolution (prolate and oblate spheroids). The model can be applied for describing blood vessels in a tissue, red blood cells in the blood, marrow within trabecular bones, etc. The time dependence of the dephasing function connected with the spins inside of the objects, s_i, is shown to be expressed by Fresnel functions and creates a powder-type signal in the frequency domain. The short-time regime of the dephasing function for spins outside the objects, s_e, is always characterized by Gaussian time dependence, $s_e \sim \exp[-\zeta k(t/t_c)^2]$, with ζ being a volume fraction occupied by the objects, t_c being a characteristic dephasing time, and the coefficient k depending on the ellipsoid's shape through the aspect ratio of its axes (a/c). The long-time asymptotic behavior of s_e is always "quasispherical"-linear exponential in time, $s_e \sim \exp(-\zeta C t/t_c)$, with the same "spherical" decay rate for any ellipsoidal shape. For long prolate spheroids $(a/c) \ll 1$, there exists an intermediate characteristic regime with a linear exponential time behavior and an aspect-ratio-dependent decay rate smaller than $(\zeta C/t_c)$.   © 2001 Academic Press

Key Words: magnetic resonance; MRI; fMRI; susceptibility; blood; bone.

INTRODUCTION

It is well known that magnetic inhomogeneities play a significant role in the process of magnetic resonance signal evolution, and an analysis of this phenomenon is one of the classic topics of magnetic resonance theory (*1*). Magnetic inhomogeneities can be of different origin, size, etc., and they affect the NMR signal relaxation in different ways, some of them being undesirable with others bringing useful information about the system under investigation. In application to MRI, these inhomogeneities can be roughly divided into three categories: macroscopic, mesoscopic, and microscopic, according to their relative size scale (*2*). *Macroscopic* scale refers to magnetic field changes over distances that are larger than the imaging voxel. *Microscopic* scale refers to changes in magnetic field over distances that are comparable to atomic or molecular size, i.e., over distances many

orders of magnitude smaller than the voxel size. *Mesoscopic* scale refers to distances that are much smaller than the voxel size but much bigger than the atomic and molecular scale. Mesoscopic magnetic field inhomogeneities originate from internal, tissue-specific sources, and hence could provide important information on biological tissue structure and function.

While at the earlier stages of NMR development most of the efforts were concentrated on the spin echo (SE) signal evolution, recent developments in MRI have focused mostly around free-induction decay (FID) signals. Major areas of interest have developed from important discoveries in functional MRI (*3, 4*) and MRI of trabecular bone (*5, 6*). For example, in the case of blood oxygenation level-dependent (BOLD) contrast in MRI, paramagnetic deoxyhemoglobin in venous blood creates a mesoscopic inhomogeneous magnetic field in the tissue surrounding the blood vessel network. This inhomogeneous field causes FID NMR signal dephasing. Numerous attempts to quantitate the blood oxygenation level and trabecular bone structure rely on different theoretical models of NMR signal dephasing (*7–16*). In all these theoretical models an imaging voxel was described in the framework of a two-compartment model, according to which the magnetized objects (blood vessel, etc.) occupying a volume fraction, ζ, with a magnetic susceptibility, χ_i, are embedded in a given media (tissue matrix) with a magnetic susceptibility, χ_e.

Traditionally, it was assumed that the presence of magnetized objects modifies the time dependence of the FID NMR signal by a factor $\exp(-R_2't)$ (Lorentzian signal shape),

$$S(t) = S_0(t) \exp(-R_2't), \qquad [1]$$

where $S_0(t)$ is a signal that would exist in a media free of objects. However, the theoretical consideration (*9*) predicted a non-Lorentzian behavior of the FID signal for those objects that can be modeled as randomly spatially distributed spheres, parallel infinitely long cylinders, or infinitely long cylinders with randomly distributed axis directions. In the short-time interval the signal modification factor is proportional to $\exp(-A^*t^2)$,

$$S(t) = S_0(t) \exp(-A^*t^2), \qquad [2]$$

107

whereas only in the long-time interval can the signal decay be described in terms of the R_2' relaxation rate constant equal to

$$R_2' = C\zeta/t_c, \quad t_c = [4\pi\gamma(\chi_i - \chi_e)H_0]^{-1}. \quad [3]$$

In Eq. [3] γ is a nuclear gyromagnetic ratio and H_0 is an external magnetic field. The parameter C is a numerical factor depending on the geometry of the magnetized objects. It is equal to 0.409 for spheres and $^1/_3$ for randomly distributed infinitely long cylinders (note that the numeric coefficient in the characteristic time t_c in [3] is defined slightly different to that in Ref. (9)). These theoretically predicted values of the coefficient C are in a good agreement with the results of Monte Carlo simulations (7, 8, 10, 12) for different geometrical structures. It should also be mentioned that the result of Refs. (10, 12) confirm an important conclusion of the theoretical analysis (9) that in the static dephasing regime the constant C does not depend on cylinders' or spheres' radii.

The Gaussian relaxation rate constant A^* also depends on the objects' geometry and the characteristic time t_c (9). It was hypothesized and proved with phantom (2) and *in vivo* (17) studies that an analysis of this non-Lorentzian FID signal shape can provide important information on tissue structure. However, real biological objects (blood vessels, for example) cannot be precisely described as infinitely long cylinders or spheres. A better model for blood vessels, in particular, should take into consideration the finite size of their straight segments. This is an important issue since both A^* [2] and R_2' [3] depend strongly on the objects' geometry.

We will demonstrate in this paper that for objects of arbitrary geometry there generally exist not two but three different time regimes: (1) Gaussian regime similar to [2] for short times when only nuclei closed to objects give contribution to the FID signal dephasing, (2) first Lorentzian regime similar to [3] with parameters depending on the objects' geometry (here mainly nuclei that are at distances not exceeding the largest object's size, hence "sensing" objects' shape, give contribution to the signal dephasing, and (3) second Lorentzian, or "spherical" regime (here mainly nuclei that are at distances much bigger than the largest object's size, hence "sensing" objects as point dipoles or spheres, give contribution to the signal dephasing).

To be able to extract the information on a tissue structure, details of the FID signal should be elucidated. Herein we will establish a quantitative relationship between a FID signal envelope and the objects' geometry in the framework of statistical approach (9) for magnetized objects that can be modeled by ellipsoids of revolution usually called spheroids (prolate or oblate). They can be viewed as an ellipse rotating about one of its principal axes. Prolate spheroids ("cigars") can be considered as an approximation for modeling the geometry of blood vessels of finite size and oblate spheroids ("pancakes") as a model for red blood cells.

GENERAL THEORY

As previously demonstrated (2, 9), in many practically important cases of biological systems nuclear motion does not substantially affect dephasing of a FID signal caused by susceptibility-induced mesoscopic magnetic field inhomogeneities. In these circumstances, NMR signal dephasing due to field inhomogeneities occurs before molecular diffusion averages out the phases accumulated by different nuclear magnetic moments—the so-called *static dephasing regime* (SDR). High external magnetic field, large susceptibility difference, and large length-scale susceptibility inclusions favor the static dephasing regime (see details in Ref. (9)). For example, for the blood vessel network at $H_0 = 1.5$ T the SDR is valid if an average radius of a blood vessel $R \geq 7\ \mu$m. Typical values of R in the human brain are 3–5 μm for small capillaries, 10–50 μm and larger for venules, veins, etc. It means that diffusion phenomena do not play an important role in the NMR signal formation for the mid-to-large vessel network. For higher external field, $H_0 > 4$ T, SDR dominates for all blood vessels. In all further consideration, we assume that the criterion of validity of the SDR is satisfied.

Consider the two-compartment system consisting of a large number, $N \gg 1$, of magnetized objects of magnetic susceptibility, χ_i, embedded in a medium with another magnetic susceptibility, χ_e. We will assume that the macroscopic magnetic field, $\mathbf{H}_0$, produced by the external magnet in the media is uniform (the effects of $\mathbf{H}_0$ nonuniformity on FID signal were discussed in detail earlier (2)). The presence of the objects creates an additional inhomogeneous mesoscopic magnetic field $\delta\mathbf{H}(\mathbf{r})$:

$$\delta\mathbf{H}(\mathbf{r}) = \sum_1^N \delta\mathbf{H}_n(\mathbf{r} - \mathbf{r}_n, \Omega_n). \quad [4]$$

Here $\delta\mathbf{H}_n$ is a contribution of the nth object located at the point $\mathbf{r}_n$; the letter Ω_n denotes geometrical parameters of the objects.

In an experiment with a single broadband RF pulse followed by a readout period, the FID signal normalized to the system volume, V, may be presented as

$$S(t) = \frac{\eta}{V} \int_V \rho(\mathbf{r})\exp(-t/T_2(\mathbf{r}))\exp(-i\omega(\mathbf{r})t)\,d\mathbf{r}, \quad [5]$$

where η is a coefficient depending on external parameters (hardware sensitivity, external magnetic field, flip angle, etc.), the standard factor $\exp(-t/T_2)$ describes the dissipative relaxation mechanism, and $\rho(\mathbf{r})$ is the local spin density at a point $\mathbf{r}$. The local NMR frequency at the position $\mathbf{r}$, $\omega(\mathbf{r})$, has contributions from all objects and is equal to $\omega(\mathbf{r}) = \gamma h(\mathbf{r})$, where $h(\mathbf{r})$ is a projection of the local nuclear magnetic field, $\mathbf{h}(\mathbf{r})$, on the direction of the external field $\mathbf{H}_0$. In the Lorentzian approximation (see, e.g., Ref. (18)), which is fairly precise for isotropic liquids, $\mathbf{h}(\mathbf{r}) = \mathbf{H}_0(1 + 4\pi\chi_e/3) + \delta\mathbf{H}(\mathbf{r})$, in the medium and $\mathbf{h}(\mathbf{r}) = \mathbf{H}_0(1 + 4\pi\chi_i/3) + \delta\mathbf{H}(\mathbf{r})$ inside the objects (we assume

that the magnetic susceptibilities $\chi_{i,e}$ are small enough to ignore nonlinear in χ effects).

The integration in Eq. [5] is taken over all the medium volume, V, which includes the volume occupied by the objects, v, and the volume outside them, $V_0 = V - v$. Therefore, the total signal $S(t)$ can also be divided into two parts,

$$S(t) = S_e(t) + S_i(t), \qquad [6]$$

where the functions $S_e(t)$ and $S_i(t)$ are contributions to the signal from the regions outside and inside the objects, respectively.

The expression [5] for the NMR signal is written for the specific spatial distribution of the objects and their parameters Ω_n. In reality, it should be averaged over all possible positions of the objects in the medium and over all possible values of the parameters Ω_n, namely, their orientation in space, size, shape, and other internal degrees of freedom, if any. To average the functions S_e and S_i over $\mathbf{r}_n$, and Ω_n, we should introduce the corresponding distribution functions, $P_1(\mathbf{r}_n)$ and $P_2(\Omega_n)$. Similar to Ref. (9) we assume that the total volume fraction of the objects, ζ, is small enough to ignore their overlapping. Therefore, for a statistically random and homogeneous distribution over positions of the spheroids, the functions $P_1(\mathbf{r}_n)$ have the form

$$P_1(\mathbf{r}_n) \, d\mathbf{r}_n = \frac{d\mathbf{r}_n}{V - v_n} \simeq \frac{d\mathbf{r}_n}{V}, \qquad [7]$$

where v_n is the nth object volume, $v_n \ll V$. The averaged functions $\bar{S}_e(t)$ and $\bar{S}_i(t)$ can be written in the form

$$\bar{S}_i(t) = \eta_i \rho_i \zeta \exp\left(-t/T_2^{(i)} - i\omega_0 t\right) s_i(t),$$
$$\bar{S}_e(t) = \eta_e \rho_e (1 - \zeta) \exp\left(-t/T_2^{(e)} - i\omega_0 t\right) s_e(t). \qquad [8]$$

Here $\zeta = v/V$ is the volume fraction of the objects in the system under consideration, ρ_i and ρ_e are the spin density inside and outside the objects, respectively (in our calculations the spins inside and outside the objects are assumed to be distributed uniformly). The frequency $\omega_0 = \gamma H_0(1 + 4\pi \chi_e/3)$ will be considered as the frequency of the rotating frame, and all results will be presented with respect to this reference frequency. The dimensionless normalized factors $s_i(t)$ and $s_e(t)$ determining contributions to the signal relaxation due to dephasing of spins inside and outside objects have the form

$$s_i(t) = \int \frac{P_2(\Omega)}{v(\Omega)} \, d\Omega \int_{V_i} d\mathbf{r} \exp[-i\delta\omega_i(\mathbf{r}, \Omega)t], \qquad [9]$$

$$s_e(t) = \left[\int P_2(\Omega) \, d(\Omega) \left(1 - \frac{1}{V} \right. \right.$$
$$\left. \left. \times \int_{V_e} d\mathbf{r}\{1 - \exp[-i\delta\omega_e(\mathbf{r}, \Omega)t]\} \right) \right]^N, \qquad [10]$$

where $\delta\omega_{i,e}(\mathbf{r}, \Omega)$ is the frequency shift (with respect to the basic frequency ω_0) inside and outside an object with the parameters Ω. The spatial integration in Eqs. [9] and [12] is over the region inside (V_i) and outside (V_e) a single object, respectively. Below we will refer to the $s_i(t)$ and $s_e(t)$ as internal and external dephasing functions, respectively. In the statistical limit $N \to \infty$, $V \to \infty$, $N/V = \text{const}$, the external dephasing function can be written as

$$s_e(t) = \exp[-\zeta f(t, \Omega)] \qquad [11]$$

$$f(t, \Omega) = \int \frac{d\Omega}{v(\Omega)} \int_{V_e} d\mathbf{r}\{1 - \exp[-i\delta\omega_e(\mathbf{r}, \Omega)t]\}. \qquad [12]$$

FREQUENCY SHIFT INDUCED BY SPHEROIDS

Equations [8]–[12] are rather general and can be applied to any two-compartment system (with the restrictions mentioned above). Further progress can be achieved if the objects' shape is specified. If an object of arbitrary shape is placed in a uniform applied magnetic field, $\mathbf{H}_0$, a magnetic field $\mathbf{H} = \mathbf{H}_0 + \delta\mathbf{H}$ inside and outside the object, and, consequently, the frequency shifts $\delta\omega_{i,e}(\mathbf{r}, \Omega) = \gamma[h^{(i,e)}(\mathbf{r}, \Omega) - h_0]$ will vary in magnitude and direction throughout the media in a complicated manner according to the Maxwell equations. In some special cases, field distributions can be found analytically; for example, expressions for a magnetic field distortion created by a magnetized sphere or infinitely long cylinder are well known and can be found in textbooks.

In the present paper we consider more general geometric bodies, namely, ellipsoids of revolution (spheroids), for which the field distribution can also be found in an analytical form. The models of spheres and infinitely long cylinders are particular cases of spheroids and can be obtained from the present model in the corresponding limits.

The magnetic field inside the arbitrarily oriented spheroids has been discussed in the literature on numerous occasions. As shown by Maxwell (19), a magnetic field, $\mathbf{H}^{(i)}$, inside a homogeneous ellipsoid is uniform, although its direction is not necessarily the same as the external field, $\mathbf{H}_0$. An elegant approach to this calculation can be found, for example, in Ref. (20). Here we exploit a similar approach to calculate a distribution of the inhomogeneous magnetic field outside the spheroids.

The static magnetic field created by any magnetized object can be found by solving the Laplace equation for the magnetic potential, Φ,

$$\mathbf{H} = -\nabla\Phi, \quad \nabla^2\Phi = 0, \qquad [13]$$

with the standard boundary conditions on the ellipsoid's surface, namely, continuity of the potential and the normal component of the magnetic induction

$$\Phi^{(i)} = \Phi^{(e)}, \quad B_n^{(i)} = B_n^{(e)} \qquad [14]$$

(hereafter the upper indices (i) and (e) will refer to functions inside and outside the ellipsoid, respectively). Such a problem can be solved in the case when the body surface coincides with one of the coordinate surfaces in one or another curvilinear coordinate system. For general ellipsoids, it is the ellipsoidal coordinates, and for the particular case of interest, it is the spheroidal coordinates $\{\sigma, \tau, \varphi\}$ that are connected with Cartesian coordinates by the relationships

$$
\begin{aligned}
x &= l[(\sigma^2 \pm 1)(1 - \tau^2)]^{1/2} \cos \varphi, \\
y &= l[(\sigma^2 \pm 1)(1 - \tau^2)]^{1/2} \sin \varphi, \qquad [15] \\
z &= l\sigma\tau.
\end{aligned}
$$

Hereafter the signs "+" and "−" correspond to the oblate and prolate spheroidal coordinates, respectively. These coordinates cover the space by a manifold of confocal spheroids with the distance between foci, $2l$, lying on the Z axis for prolate spheroidal coordinates and in the plane perpendicular to the Z axis for oblate spheroidal coordinates.

The parameters σ, τ, φ are defined in the intervals

$$
1 \le \sigma \le \infty, \quad -1 \le \tau \le 1, \quad 0 \le \varphi \le 2\pi \qquad [16]
$$

for prolate spheroidal coordinates, and

$$
0 \le \sigma \le \infty, \quad -1 \le \tau \le 1, \quad 0 \le \varphi \le 2\pi \qquad [17]
$$

for oblate spheroidal coordinates.

The coordinate surfaces, $\sigma = \text{const}$, are given by

$$
\frac{x^2 + y^2}{l^2(\sigma^2 \pm 1)} + \frac{z^2}{l^2\sigma^2} = 1. \qquad [18]
$$

The parameter σ "numerates" the spheroids by defining their size. Parameters τ and φ define a position on the surface [18] (φ is an azimuth angle and τ is an analogue of $\cos\theta$ in the spherical coordinates).

Let us consider a spheroid obtained by rotating an ellipse with half-axes a and c about the c axis. If we want the surface of this spheroid to coincide with one of the coordinate surfaces, we should adjust the foci of the coordinate system with those of the given spheroid, i.e., orient the rotation axis along the Cartesian axis Z and put $l = |a^2 - c^2|^{1/2}$. In the case of the given prolate, $c > a$, and oblate, $c < a$, spheroids, its surface coincides with the coordinate surface

$$
\sigma = \sigma_0 =
\begin{cases}
[1 - (a/c)^2]^{-1/2}, & c = l\sigma_0, \\
\quad a = l(\sigma_0^2 - 1)^{1/2}, & c > a \\
[(a/c)^2 - 1]^{-1/2}, & c = l\sigma_0, \\
\quad a = l(\sigma_0^2 + 1)^{1/2}, & c < a.
\end{cases} \qquad [19]
$$

The space inside and outside the spheroid corresponds to $\sigma < \sigma_0$ and $\sigma > \sigma_0$, respectively.

The limiting case of the sphere can be reached by putting $\sigma_0 \to \infty$, $l \to 0$, $\sigma_0 l = \text{const}$ for both prolate and oblate spheroids. In the case $\sigma_0 \to 1$, $l \to \infty$, $l(\sigma_0^2 - 1)^{1/2} = \text{const}$ a prolate spheroid degenerates into an infinitely long cylinder. The case $\sigma_0 \to 0$ for oblate spheroids corresponds to an infinite plate.

Because of the axial symmetry about the Z axis, we can assume without loss of generality that the applied magnetic field, $\mathbf{H}_0$ lies parallel to the XZ plane of the Cartesian coordinate system,

$$
\mathbf{H}_0 = (H_{0x}, 0, H_{0z}) = (H_0 \sin\alpha, 0, H_0 \cos\alpha). \qquad [20]
$$

The Laplace equation in the spheroidal coordinates has the form

$$
\frac{\partial}{\partial\sigma}\left[(\sigma^2 \pm 1)\frac{\partial\Phi}{\partial\sigma}\right] + \frac{\partial}{\partial\tau}\left[(1 - \tau^2)\frac{\partial\Phi}{\partial\tau}\right]
$$
$$
+ \frac{(\sigma^2 \pm \tau^2)}{(\sigma^2 \pm 1)(1 - \tau^2)}\frac{\partial^2\Phi}{\partial\varphi^2} = 0. \qquad [21]
$$

Solving this equation with the boundary conditions [14] (see the details in Appendix A), the frequency shifts $\delta\omega_e$ outside the spheroid can be written as a function of the spheroidal coordinates $\{\sigma, \tau, \varphi\}$ and the angle α,

$$
\delta\omega_\pm^{(e)} = \delta\omega_s \sigma_0 (\sigma_0^2 \pm 1) h_\pm^{(e)}(\sigma, \tau, \varphi; \alpha). \qquad [22]
$$

Here

$$
\delta\omega_s = 1/t_c = 4\pi\gamma H_0(\chi_i - \chi_e) \qquad [23]
$$

is the characteristic frequency shift,

$$
\begin{aligned}
h_+^{(e)} &= \cos^2\alpha\left(\cot^{-1}\sigma - \frac{\sigma}{\sigma^2 + \tau^2}\right) + \sin 2\alpha \frac{\tau\cos\varphi}{\sigma^2 + \tau^2} \\
&\times \left(\frac{1 - \tau^2}{\sigma^2 + 1}\right)^{1/2} + \sin^2\alpha\left[\frac{1}{2}\left(\frac{\sigma}{\sigma^2 + 1} - \cot^{-1}\sigma\right)\right. \\
&\left. + \frac{\sigma(1 - \tau^2)\cos^2\varphi}{(\sigma^2 + 1)(\sigma^2 + \tau^2)}\right], \qquad [24]
\end{aligned}
$$

$$
\begin{aligned}
h_-^{(e)} &= \cos^2\alpha\left(\frac{\sigma}{\sigma^2 - \tau^2} - \coth^{-1}\sigma\right) + \sin 2\alpha \frac{\tau\cos\varphi}{(\sigma^2 - \tau^2)} \\
&\times \left(\frac{1 - \tau^2}{\sigma^2 - 1}\right)^{1/2} + \sin^2\alpha\left[\frac{1}{2}\left(\coth^{-1}\sigma - \frac{\sigma}{\sigma^2 - 1}\right)\right. \\
&\left. + \frac{\sigma(1 - \tau^2)\cos^2\varphi}{(\sigma^2 - 1)(\sigma^2 - \tau^2)}\right]. \qquad [25]
\end{aligned}
$$

The frequency shift inside the spheroid can be conveniently expressed in terms of the demagnetizing factors, $n_\pm^{x,z}$

[A14]–[A15]:

$$\delta\omega_{\pm}^{(e)} = -\delta\omega_s \left[n_{\pm}^z(\sigma_0) \cos^2\alpha + n_{\pm}^x(\sigma_0) \sin^2\alpha - \frac{1}{3} \right] \quad [26]$$

(the last term in Eq. [26] accounts for the difference between the macroscopic field, B_i, and the local field in the Lorentzian approximation, see, e.g., (18)).

It is important to note that the expressions [24]–[26] depend on the spheroids' axes a and c only through the dimensionless parameter σ_0 [19], i.e., through the ratio a/c, and do not depend on the distance between its foci, l.

Thus, in the case of spheroids, the parameter Ω introduced in Eq. [4] includes three quantities describing the form and orientation of the spheroid: l, σ_0, and α, and averaging in Eqs. [9]–[10] should be done over these three quantities with appropriate distribution functions. Therefore the distribution function $P_2(\Omega)$ is a product

$$P_2(\Omega) = P_l(l) P_{\sigma_0}(\sigma_0) P_\alpha(\alpha), \quad [27]$$

where $P_l(l)$, $P_{\sigma_0}(\sigma_0)$, and $P_\alpha(\alpha)$ are the distribution functions for the distance between the spheroid's foci, the spheroid's shape, and the angle between its rotation axis and the external magnetic field. The distribution function $P_{\sigma_0}(\sigma_0)$ depends on particulars of the system. In this paper we restrict ourselves to the case in which all the spheroids are similar, i.e., have the same ratio of the half-axes, $(a/c) = $ const. In this particular case, the parameter σ_0 is fixed.

For a random uniform distribution of the spheroids' axes directions (see, e.g., Ref. (3)),

$$P_\alpha(\alpha) = \frac{\sin\alpha}{2}, \quad 0 \le \alpha \le \pi. \quad [28]$$

As mentioned above, the space inside and outside the spheroid corresponds to $\sigma < \sigma_0$ and $\sigma > \sigma_0$, respectively. The frequency shift inside the spheroid is described by Eq. [26] and does not depend on coordinates. The internal dephasing function $s_i(t)$ [9] takes the form

$$s_i^{\pm}(t) = \int_0^\pi d\alpha \frac{\sin\alpha}{2} \exp\left\{ -i\psi \left[n_{\pm}^z(\sigma_0) \cos^2\alpha \right.\right.$$
$$\left.\left. + n_{\pm}^x(\sigma_0) \sin^2\alpha - \frac{1}{3} \right] \right\}, \quad [29]$$

where

$$\psi = \delta\omega_s t. \quad [30]$$

The external dephasing function $s_e(t)$ [11], describing the contribution of the media outside the spheroids, can be written as

$$s_e^{\pm}(t) = \exp[-\zeta f_{\pm}(\sigma_0, t)], \quad [31]$$

$$f_{\pm}(\sigma_0, t) = \frac{3}{4\pi\beta} \int_0^\pi d\alpha \frac{\sin\alpha}{2} \int_{\sigma_0}^\infty d\sigma \int_{-1}^1 d\tau \int_0^{2\pi} d\varphi (\sigma^2 \pm \tau^2)$$
$$\times \{1 - \exp[-i\psi\beta h_{\pm}^{(e)}(\sigma, \tau, \varphi; \alpha)]\}, \quad [32]$$

where

$$\beta = \sigma_0(\sigma_0^2 \pm 1) = \left(\frac{a}{c}\right)^2 \left| 1 - \left(\frac{a}{c}\right)^2 \right|^{-3/2}. \quad [33]$$

When writing Eq. [32], we took into account that the volume element dV in the spheroidal coordinates is equal to

$$dV = l^3(\sigma^2 \pm \tau^2) d\sigma \, d\tau \, d\varphi, \quad [34]$$

and the volume of the spheroid with the half-axes a and c is

$$v = \frac{4\pi}{3} a^2 c = \frac{4\pi}{3} l^3 \sigma_0(\sigma_0^2 \pm 1) = \frac{4\pi}{3} l^3 \beta. \quad [35]$$

It should be noted that for a given volume fraction, ζ, the functions $s_{i,e}(t)$ do not depend on the distribution function $P_l(l)$. Just the same situation takes place for the particular cases of spheres and infinitely long cylinders considered in Ref. (9). This is a result of the general scaling law valid for the static dephasing regime (21). As mentioned in the Introduction, for the particular case of spherical and cylindrical objects, the independence of gradient echo relaxivity (in fact, the function $f(t)$) from objects' size in the static dephasing regime has been confirmed both experimentally and by the Monte Carlo simulations in Refs. (10, 12).
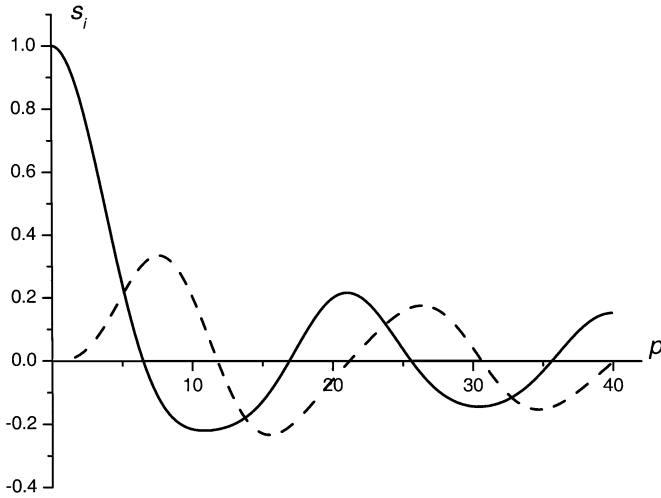
THE INTERNAL DEPHASING FUNCTION $s_i(t)$

Let us begin by analyzing the function $s_i(t)$. Taking into account the identity $2n_{\pm}^x + n_{\pm}^z = 1$, it is easy to see that $s_i(t)$ depends on time and demagnetizing factor of the spheroid only in the combination

$$p(t) = \psi(n_{\pm}^x - n_{\pm}^z) = (\delta\omega_s t)(1 - 3n_{\pm}^z)/2. \quad [36]$$

The integral in Eq. [29] can be expressed in terms of Fresnel functions $C(x)$ and $S(x)$ (see, e.g., Ref. (22)),

$$s_i(t) = s_i(p(t)) = \left(\frac{\pi}{2|p|}\right)^{1/2} \exp(ip) \left[C(|p|^{1/2}) \right.$$
$$\left. - i \, \text{sgn}(p) S(|p|^{1/2}) \right]. \quad [37]$$

FIG. 1. The real (solid line) and imaginary (dashed line) parts of the internal dephasing function s_i [37]. The parameter p is proportional to the FID time, t, and is defined by Eq. [36].

It can be easily verified that the real part of $s_i(t)$ is an even whereas the imaginary part is an odd function of p. The real and imaginary parts of the function s_i are shown in Fig. 1 for the case $p > 0$.

Note, in the degenerate case of spheres, $n_\pm^x = n_\pm^z = 1/3$, $p \equiv 0$. In this case, apparently, spins inside all objects (spheres) have the same frequency. Moreover, the local field in the Lorentzian approximation coincides with the local field in the external media, h_0, and the frequency shift is absent; hence, no signal dephasing occurs, $s_i(t) = 1$.

The asymptotic forms of the function [37] are

$$s_i \approx \begin{cases} 1 - \frac{2}{45}p^2 + i\frac{8}{2835}p^3, & p \ll 1, \\ \frac{1}{2}\left(\frac{\pi}{|p|}\right)^{1/2}\exp\left[i\cdot\left(\frac{p}{3} - \frac{\pi}{4}\operatorname{sgn}p\right)\right], & |p| \gg 1. \end{cases} \quad [38]$$

In the particular case of infinitely long cylinders, for which $n_-^x = 1/2$, $n_-^z = 0$, the asymptotic expressions [38] coincide with those obtained in Ref. (14) with the exception of the coefficient at ip^3 due to a misprint in Ref. (14) (private communication with V. Kiselev).

As $s_i(t)$ is a universal function and depends on t only through the parameter p, the time dependence of the signal produced by spheroids of different shape differs only in a time scale. For example, for spheroids close to spherical, when $|n_\pm^x - n_\pm^z| \ll 1$, the small-$p$ range takes place for very long real time, $\delta\omega_s t \sim |n_\pm^x - n_\pm^z|^{-1} \gg 1$, and this range tends to infinity for a pure sphere.

THE EXTERNAL DEPHASING FUNCTION $s_e(t)$

Equations [31] and [32] describe the signal attenuation due to the spin dephasing outsides the spheroids. For the short time scale, when $\psi = \delta\omega_s t \ll 1$, the exponent in Eq. [32] can be expanded in series and, with accuracy to ψ^2, all the integrals in Eq. [32] can be taken exactly. The real part of the functions $f_\pm(\sigma_0, t)$ for the prolate (f_-) and oblate (f_+) spheroids turn out to be proportional to t^2,

$$\operatorname{Re}[f_\pm(\sigma_0, t)] = k_\pm(\sigma_0)(\delta\omega_s t)^2 + O(\delta\omega_s t)^4, \quad [39]$$

$$k_-(\sigma_0) = \frac{\sigma_0}{30}\left[\sigma_0(4-3\sigma_0^2) + 2(\sigma_0^2-1)(3\sigma_0^2-2)\right.$$
$$\left. \times \coth^{-1}\sigma_0 - 3\sigma_0(\sigma_0^2-1)^2(\coth^{-1}\sigma_0)^2\right], \quad [40]$$

$$k_+(\sigma_0) = \frac{\sigma_0}{30}\left[-\sigma_0(4+3\sigma_0^2) + 2(\sigma_0^2+1)(3\sigma_0^2+2)\right.$$
$$\left. \times \cot^{-1}\sigma_0 - 3\sigma_0(\sigma_0^2+1)^2(\cot^{-1}\sigma_0)^2\right], \quad [41]$$

whereas its imaginary part is negligibly small, $\operatorname{Im}[f_\pm(\sigma_0, t)] = O(\psi^3)$. Such a behavior of the function f is similar to that for the models of spheres and cylinders considered in (9).

The coefficients $k_\pm(\sigma_0)$ have the following asymptotic form (recalling that for the oblate spheroids $0 < \sigma_0 < \infty$, and for the prolate spheroids $1 < \sigma_0 < \infty$):

$$k_-(\sigma_0) = \begin{cases} \frac{1}{30} + \left(\frac{\sigma_0-1}{15}\right)\left[-2 + \ln\frac{2}{(\sigma_0-1)}\right], \\ \quad (\sigma_0 - 1) \ll 1 \ (c \ll a), \\ \frac{2}{45} - \frac{2}{1125\sigma_0^4} - \frac{4}{2625\sigma_0^6}, \\ \quad \sigma_0 \gg 1 \ (a \to c), \end{cases} \quad [42]$$

$$k_+(\sigma_0) = \begin{cases} \frac{\pi\sigma_0}{15} - \frac{(3\pi^2 + 32)\sigma_0^2}{120}, & \sigma_0 \ll 1 \ (a \ll c), \\ \frac{2}{45} - \frac{2}{1125\sigma_0^4} + \frac{4}{2625\sigma_0^6}, & \sigma_0 \gg 1(c \to a). \end{cases} \quad [43]$$

As a function of the spheroid half-axes ratio (a/c), the coefficient k in Eq. [39] is a single function, the intervals $0 < (a/c) < 1$ and $1 < (a/c) < \infty$ referring to the prolate and oblate spheroids, respectively (see Eq. [19]). The dependence $k = k(a/c)$ is shown in Fig. 2. At the point $(a/c) = 1$ $(\sigma_0 \to \infty)$, corresponding to the limiting case of sphere, the function $k(a/c)$ has a maximum $k_{max} = 2/45$, and in the limit $(a/c) \to 0$ $(\sigma_0 \to 1)$, when the prolate spheroid elongates into an infinitely long cylinder, the coefficient $k = 1/30$, which coincides (however, note difference in notation) with the results obtained in Ref. (9). If the ratio $(a/c) \to \infty(\sigma_0 \to 0)$, the oblate spheroid degenerates into an infinite plate, and $k_+ \to 0$.

In the long-time regime, when $\psi \gg 1$, we consider first the case $\sigma_0 \gg 1$, which corresponds to nearly spherical objects. For spin outside the objects ($\sigma \geq \sigma_0 \gg 1$), the functions $h_\pm^{(e)}(\sigma, \tau, \varphi; \alpha)$ in Eqs. [24] and [25] can be substantially
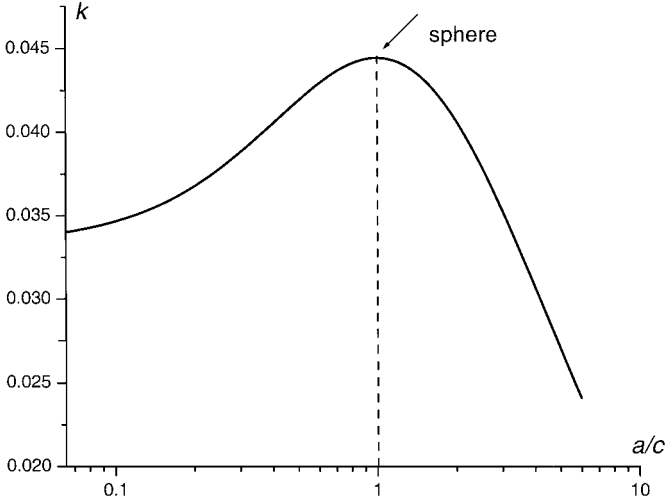
FIG. 2. The coefficient k [39] defining a short-time (quadratic) behavior of the external dephasing function ($s_e = \exp[-\zeta k(\delta\omega_s t)^2]$) as a function of the aspect ratio (a/c).

simplified,

$$h_\pm^{(e)}(\sigma, \tau, \varphi; \alpha) = \frac{1}{\sigma^3}\left\{\frac{1}{3} - \left[\tau\cos\alpha + (1-\tau^2)^{1/2}\sin\alpha\cos\varphi\right]^2\right\}$$
[44]

(in fact, this approximation is valid already for $\sigma \geq 2$). Substituting Eq. [44] into the intergral [32] and integrating over α and φ, we get

$$f_\pm(\sigma_0, t)$$
$$= \frac{3}{\beta}\int_0^1 du \int_{\sigma_0}^\infty \sigma^2 d\sigma\left\{1 = \exp\left[-i\frac{\psi\beta}{\sigma^3}\left(\frac{1}{3}-u^2\right)\right]\right\}. \quad [45]$$

Calculating the intergral [45] for $\psi \gg 1$, $\beta \gg 1$ we obtain

$$f_\pm(\sigma_0, t) \simeq f_s(t) = C_1\psi - 1 - iC_2\psi,$$
$$C_1 = \frac{2\pi}{9\sqrt{3}} \simeq 0.403, \quad C_2 \simeq 0.053. \quad [46]$$

Such an asymptotic behavior exactly coincides with the result of Ref. (9) for the model of spheres.

An asymptotic expression similar to Eq. [46] can also be obtained for an arbitrary β (Eq. [33]) in the long-time limit $\beta\psi \gg 1$. A comparison with numerical calculations shows that the function $f(\sigma_0, t)$ can be approximated by a straight line with the same slope $C_1 = 0.403$ but with a constant depending on σ_0:

$$f_\pm(\sigma_0, t) \simeq C_1\psi - \frac{C_3}{\sigma_0(\sigma_0^2 \pm 1)} - 1 - iC_2\psi, \quad C_3 \simeq 0.04. \quad [47]$$

In the case $\beta \geq 1$ the asymptotic behavior [47] takes place for any $\psi \gg 1$. However, due to the smallness of the coefficient C_3, the second term in Eq. [47] essentially contributes only for sufficiently small β (long "cigars," for which $\beta \approx 2(\sigma_0-1) \ll 1$, or thin "pancakes," for which $\beta \approx \sigma_0 \ll 1$). In the case $\beta \ll 1$, there exists an intermediate time interval,

$$\psi = \delta\omega_s t \gg 1, \quad \beta\psi \ll 1. \quad [48]$$

Let us consider the case of the prolate spheroids with $\sigma_0 \to 1$ (long "cigars"). It can be shown that in this limit the integral in Eq. [32] is mainly contributed by the interval of σ close to 1, and the function $h_-^{(e)}$[25] can be approximated by

$$h_-^{(e)} \simeq \frac{\sin^2\alpha}{4(\sigma-1)}\cos 2\varphi\left[1 + O\left((\sigma-1)^{1/2}\right)\right]. \quad [49]$$

Substituting Eq. [49] into Eq. [32], we obtain after integration

$$f_-(\sigma_0, t) \simeq f_c(t) = {}_1F_2\left(-\frac{1}{2}; \left\{\frac{3}{4}, \frac{5}{4}\right\}; -\frac{\psi^2}{16}\right) - 1, \quad [50]$$

where ${}_1F_2(\alpha; \{\beta, \gamma\}; x)$ is the so-called generalized hypergeometric function. This function is not in common use; therefore we provide its definition and some properties in Appendix B. The expression [50] does not depend on the parameter σ_0 and, in fact, describes the limiting case $\sigma_0 = 1$, corresponding to an infinitely long cylinder. Its asymptotic behavior, which can be obtained by using Eq. [B3], coincides with that given in Ref. (9) for the model of randomly oriented cylinders:

$$f_c(t) \simeq \begin{cases} \frac{\psi^2}{30}, & \psi \ll 1, \\ \frac{\psi}{3} - 1, & \psi \gg 1. \end{cases} \quad [51]$$

The short-time asymptote of the function $f_c(t)$ coincides with the cylindrical limit ($\sigma_0 = 1$) of the expression [42].

However, the behavior of the function $f_-(\sigma_0, t)$ even for rather small values of $(\sigma_0 - 1) \sim 10^{-3}$ ($a/c \sim 1:20$) differs substantially from that of $f_c(t)$. We fitted the numerical results for several values of $\sigma_0(\sigma_0-1 = (1 \div 5)\cdot 10^{-3})$ at the interval $30 < \psi < 80$ to the straight lines

$$f_-(\sigma_0, t) \simeq k_1(\sigma_0)\psi - k_2(\sigma_0), \quad [52]$$

and obtained the following interpolation formulas for the coefficients $k_{1,2}(\sigma_0)$,

$$k_1(\sigma_0) \simeq \frac{1}{3} + 0.62(\sigma_0 - 1)^{1/2},$$
$$k_2(\sigma_0) \simeq 1 + 10(\sigma_0 - 1)^{1/2}. \quad [53]$$

Thus, for the spheroid with a small aspect ratio (long "cigars") we can distinguish three characteristic time intervals of different

behavior of the function $f_-(\sigma_0, t)$:(A)$\psi \leq 1$, where $f_- \sim t^2$ (see Eq. [39]); (B) $1 \ll \psi \leq 1/\beta$, where the cylinder-like approximation [52] takes place; and (C) $\psi \gg 1/\beta$, where the function f_- is described by the sphere-like expression [47]. The transition between the intervals (A) and (B) takes place at $\psi = \delta\omega_s t \approx 4.5$ practically regardless of the parameter σ_0. The transition between the intervals (B) and (C) takes place at the characteristic time, $t_{cs} \approx (\beta \cdot \delta\omega_0)^{-1}$. This time increases as the aspect ratio of the spheroids, (a/c), decreases, $t_{cs} \to \infty$ when $\sigma_0 \to 1$, and for pure infinitely long cylinders the interval (C) does not exist. Although the sphere-like interval (C) exists for any finite value of the parameter σ_0, if the intrinsic time, T_2, is much less than the characteristic time, t_{cs}, only the cylinder-like behavior of the function $f_-(\sigma_0, t)$ can be observed. When the ratio (a/c) increases, the characteristic time t_{cs} decreases, and for $\sigma_0 \sim 1.05$ the intermediate interval (B) practically vanishes. All the three characteristic time intervals can be observed for some intermediate values of the parameter σ_0.

A general picture of the time dependence of the real part of the function $f_-(\sigma_0, t)$ is shown in Fig. 3 for the prolate spheroid with $\sigma_0 = 1.002$, $(a/c \approx 1:16)$, 1.01 $(a/c \approx 1:7)$, and $1.04(a/c \approx 1:3.6$. The difference in the slope between the curves varies in the interval between $\frac{1}{3}$ (infinite cylinder, dashed line in Fig. 3) and 0.4 (spherical asymptote, dotted line). A detailed analysis shows that in the interval $10 < \psi < 100$ curve 1, corresponding to the small value $\sigma_0 = 1.002$, can be approximated by the straight line with the parameters characteristic to the cylinder-like interval (B) [52], whereas curve 3, corresponding to $\sigma_0 = 1.04$, is described at the same interval by the sphere-like asymptote [47] (interval (C)) and is parallel to the dotted line corresponding to the spherical limit [46]. Both intervals (B) and (C) are present for the curve 2, corresponding to the
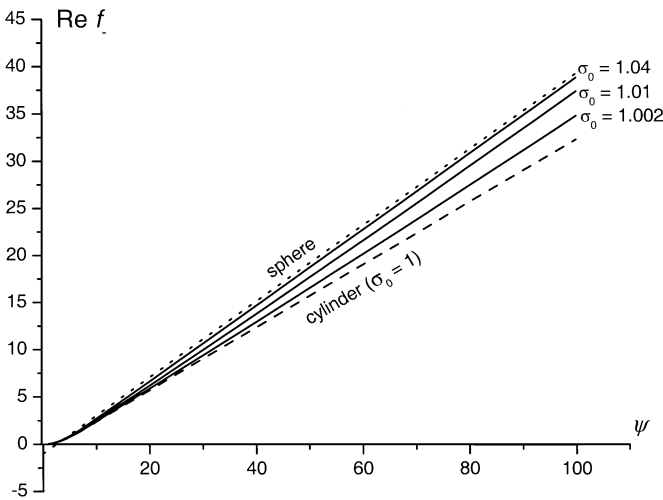
FIG. 3. The real part of the function f_- [32] defining the external dephasing function $s_e^- = \exp[-\zeta f_-(t)]$ for the spheroids with different aspect ratio: $a/c = 1:16$ ($\sigma_0 = 1.002$), $a/c = 1:7$ ($\sigma_0 = 1.01$), and $a/c = 1:3.6$ ($\sigma_0 = 1.04$). The dashed line represents the cylindrical approximation f_c [50]; the dotted line represents the spherical asymptote [46]; $\Psi = \delta\omega_s t$.

intermediate value $\sigma_0 = 1.01$: in the interval $10 < \psi < 40$ it can be approximated by the cylinder-like straight line [52], and in the interval $60 < \psi$ its behavior is described by the sphere asymptote [47].

For the oblate spheroids, the characteristic behavior of the dephasing function $f_+(\sigma_0, t)$ in the interval (B) described above does not take place because, in contrast to an infinitely long cylinder, an infinite plate (the limiting case of the "pancakes," $\sigma_0 \to 0$) does not create any inhomogeneous field distortion.

CONCLUDING REMARKS

In the previous sections we presented specific features of the external dephasing function by modeling the inclusions as spheroidal objects. However, some important features of the behavior of this function take place for objects of arbitrary geometry.

First, in the short-time regime, the dependence of the external function, $s_e(t)$, which provides the main contribution to the total dephasing of the signal, is similar to Eq. [39] for any object of a finite size. Indeed, for a sufficiently small time, the exponent in the integrand in Eq. [12] can be expanded into series, and the first nonzero real term is quadratic in t, which gives the dependence $\text{Re}[s_e(t)] \sim t^2$ (the only exception is a model of point dipoles, considered in Ref. (1), for which the field created by a dipole tends to infinity when approaching the dipole, and the exponent cannot be expanded in a series).

The long-time asymptotic behavior of the dephasing function $s_e(t)$, similar to the sphere-like dependence [47], is also characteristic to object of any geometry. To explain it, let us consider one object (spheroid, for example), creating outside its boundaries an inhomogeneous magnetic field distortion affecting the precessing spins. At $t = 0$ all spins start precession with the same phase, but due to inhomogeneity of the magnetic field, this begins to dephase; once a phase difference between two spins achieves π, we can make the approximation that these two spins no longer contribute to the total signal. A time needed to break the coherent precession of two spins is on the order of $t_b \sim \pi/\delta\omega$, where $\delta\omega$ is the frequency shift between the spins, $\delta\omega = \gamma \cdot \delta H$. As the field distortion, δH, created by the object, decreases with a distance from the latter, the corresponding dephasing time t_b increases, and the dephasing process can be considered as a outward propagating wave of peculiar kind, which can be called "a dephasing wave." The dephasing-induced signal damping is proportional to the volume fraction covered by this wave and is described by the function $f(t, \Omega)$ introduced by the expression [12]. In the system consisting of many objects, each of them can be considered as a source of one dephasing wave, and the regions covered by different waves overlap. In the case of randomly distributed objects with sufficiently small volume fraction, $\zeta \ll 1$, this overlapping can be readily taken into account by means of the simple probability approach and is described by the exponent $\exp[-\zeta f]$ similar to that in Eq. [11].

In the beginning of the dephasing process, the dephasing wave propagation strongly depends on the specific object geometry. However, when the wave covers the volume much larger than that of the object, all of the increase of the covered volume is due to regions far from the object. The field distortion created by the object at long distance does not depend on the object geometry and is the same as for a sphere or a point dipole. Consequently, in the long-time limit, $t > t_{cs}$ (t_{cs} is some characteristic time), the increase of the function $f(t)$ (in fact, its time derivative) is the same as for the sphere model and the asymptotic behavior of $f(t)$ is similar to Eq. [47],

$$f(t) \simeq C_1 \psi - i C_2 \psi + \tilde{C}, \qquad [54]$$

where $C_{1,2}$ are given in Eq. [47] and are independent from the object geometry whereas the constant $\tilde{C}$ is geometry-dependent. It should be noted, however, that in a real experiment, this asymptotic behavior can be observed only if the relaxation time T_2 does not exceed the characteristic time, t_{cs}, which is geometry-dependent (e.g., in the case of the spheroids, the characteristic time $t_{cs} = (\beta\delta\omega_0)^{-1}$).

The results obtained demonstrate a rather complicated behavior of the NMR signal evolution, which substantially deviates from the standard exponential (T_2^*-like) decay (in particular, the system distinguishes three characteristic time intervals). They can be applied for more adequate interpretation of experimental MRI data when the magnetic resonance signal is affected by the vascular network (BOLD contrast, susceptibility contrast agent), trabecular bones, alveolar walls of the lung, or red blood cells.

Note also that a signal behavior around a spin echo time $2\tau_e$ can be obtained by substituting $t \to |t - 2\tau_e|$ in the functions $s_{i,e}$ [9]–[12].

APPENDIX A

Field Distortion Created by a Spheroid

Let us seek the solution of Eq. [21] in the form

$$\Phi = \Phi_0(x, z) - H_{0z} z F^{(z)}(\sigma) - H_{0x} x F^{(x)}(\sigma), \qquad [A1]$$

where Φ_0 is the magnetic potential corresponding to $\mathbf{H}_0$,

$$\Phi_0(x, z) = -(H_{0x} x + H_{0z} z). \qquad [A2]$$

Since Eq. [21] as well as the boundary conditions [14] are linear, we can separate equations for the functions $F^{(x)}(\sigma)$ and $F^{(z)}(\sigma)$. Substituting Eq. [A1] into Eq. [13], we obtain for the functions $F^{(x,z)}(\sigma)$ the ordinary differential equations, which can be readily solved. Taking into account that far from the spheroid $\Phi \to \Phi_0(x, z)$, i.e., $F^{(x,z)}(\sigma) \to 0$ at $\sigma \to \infty$, these solutions for the prolate (F_+) and oblate (F_-) spheroid can be written in the form

$$F_\pm^{(x,z)}(\sigma) = A_\pm^{(x,z)} I_\pm^{(x,z)}(\sigma),$$

$$I_\pm^{(x)}(\sigma) = \begin{cases} \frac{1}{2}\left(\frac{\sigma}{\sigma^2+1} - \cot^{-1}\sigma\right), \\ \frac{1}{2}\left(\coth^{-1}\sigma - \frac{\sigma}{\sigma^2-1}\right), \end{cases} \quad I_\pm^{(z)}(\sigma) = \begin{cases} \coth^{-1}\sigma - \frac{1}{\sigma}, \\ \frac{1}{\sigma} - \coth^{-1}\sigma, \end{cases}$$

$$[A3]$$

where $A_\pm^{(x,z)}$ are constants.

Thus, the magnetic potential outside the spheroid can be written as

$$\Phi_\pm^{(e)} = -l H_0 \left\{ [(\sigma^2 \pm 1)(1 - \tau^2)]^{1/2} \cos\varphi \left(1 + A_\pm^{(x)} I_\pm^{(x)}(\sigma)\right) \right.$$
$$\left. \times \sin\alpha + \sigma\tau \left(1 + A_\pm^{(z)} I_\pm^{(z)}(\sigma)\right) \cos\alpha \right\}. \qquad [A4]$$

Inside the spheroid the field is uniform and the magnetic potential is

$$\Phi_\pm^{(i)} = -\left(a_\pm^{(x)} H_{0x} x + a_\pm^{(z)} H_{0z} z\right). \qquad [A5]$$

The coefficients $A_\pm^{(x,z)}$ and $a_\pm^{(x,z)}$ can be obtained from the boundary conditions on the spheroid's surface [14]. The normal components of the magnetic induction inside and outside the spheroid are equal to

$$B_n^{(i,e)} = \mu_{i,e} H_n^{i,e} = -\mu_{i,e} g_{\sigma\sigma}^{-1/2} \frac{\partial \Phi^{(i,e)}}{\partial \sigma}, \qquad [A6]$$

where $\mu_{i,e} = 1 + 4\pi \chi_{i,e}$ are the permeability of the spheroid and the media, respectively; $g_{\sigma\sigma}$ is the $\sigma\sigma$-element of the curvature tensor, $g_{\sigma\sigma} = l^2(\sigma^2 \pm \tau^2)(\sigma^2 \pm \tau^2)^{-1}$. Substituting Eqs. [A3]–[A6] into the boundary conditions [14], we find that

$$A_\pm^{(x,z)} = \frac{\delta\mu\sigma_0(\sigma_0^2 \pm 1)}{\left[\mu_e + \delta\mu\sigma_0(\sigma_0^2 \pm 1)I_\pm^{(x,z)}(\sigma_0)\right]},$$
$$a_\pm^{(x,z)} = \frac{\mu_e}{\left[\mu_e + \delta\mu\sigma_0(\sigma_0^2 \pm 1)I_\pm^{(x,z)}(\sigma_0)\right]}, \qquad [A7]$$

where $\delta\mu = \mu_i - \mu_e = 4\pi \cdot \Delta\chi$.

In the case of para- or diamagnetic media and objects with very small susceptibilities, $\chi_{i,e} \ll 1$, we can neglect the second term in the denominators and consider

$$A_\pm^{(x)} \simeq A_\pm^{(z)} \simeq \sigma_0(\sigma_0^2 \pm 1)\delta\mu. \qquad [A8]$$

The magnetic field, corresponding to the potential $\Phi^{(e)}$, has the components

$$H_x = H_{0x} + H_{0x} x A_\pm^{(x)} \frac{\partial I_\pm^{(x)}(\sigma)}{\partial x} + H_{0z} z A_\pm^{(z)} \frac{\partial I_\pm^{(z)}(\sigma)}{\partial x},$$
$$[A9]$$
$$H_z = H_{oz} + H_{0x} x A_\pm^{(x)} \frac{\partial I_\pm^{(x)}(\sigma)}{\partial z} + H_{0z} z A_\pm^{(z)} \frac{\partial I_\pm^{(z)}(\sigma)}{\partial z}.$$

The projection of the total magnetic field on the direction of the applied field, $\mathbf{H}_0$, is equal to

$$H^{(e)} = H_x \sin\alpha + H_z \cos\alpha. \qquad [\text{A10}]$$

Substituting Eq. [A9] into Eq. [A10] and using Eqs. [15], [A3], we obtain

$$H_{\pm}^{(e)} = H_0 + \delta H_{\pm}^{(e)},$$

$$\delta H_+^{(e)} = \delta\mu H_0 \sigma_0 (\sigma_0^2 + 1)\left\{ \cos^2\alpha \left(\cot^{-1}\sigma - \frac{\sigma}{\sigma^2 + \tau^2} \right) \right.$$

$$+ \sin 2\alpha \frac{\tau\cos\varphi}{\sigma^2 + \tau^2}\left(\frac{1 - \tau^2}{\sigma^2 + 1} \right)^{1/2} + \sin^2\alpha\left[\frac{1}{2}\left(\frac{\sigma}{\sigma^2 + 1} \right.\right.$$

$$\left.\left.\left. - \cot^{-1}\sigma \right) + \frac{\sigma(1 - \tau^2)\cos^2\varphi}{(\sigma^2 + 1)(\sigma^2 + \tau^2)} \right] \right\}, \qquad [\text{A11}]$$

$$\delta H_-^{(e)} = \delta\mu H_0 \sigma_0 (\sigma_0^2 - 1)\left\{ \cos^2\alpha \left(\frac{\sigma}{(\sigma^2 - \tau^2)} - \coth^{-1}\sigma \right) \right.$$

$$+ \sin 2\alpha \frac{\tau\cos\varphi}{(\sigma^2 - \tau^2)}\left(\frac{1 - \tau^2}{\sigma^2 - 1} \right)^{1/2} + \sin^2\alpha\left[\frac{1}{2}\left(\coth^{-1}\sigma \right.\right.$$

$$\left.\left.\left. - \frac{\sigma}{\sigma^2 - 1} \right) + \frac{\sigma(1 - \tau^2)\cos^2\varphi}{(\sigma^2 - 1)(\sigma^2 - \tau^2)} \right] \right\}. \qquad [\text{A12}]$$

Using Eqs. [A3] and [A7], the uniform field distortion inside the spheroid, $\delta H_{\pm}^{(i)}$, can be written in terms of the demagnetizing factor of the ellipsoid of revolution, $n_{\pm}^{(x,z)}$,

$$\delta H_{\pm}^{(i)} = -\delta\mu\, H_0 (n_{\pm}^z \cos^2\alpha + n_{\pm}^x \sin^2\alpha), \qquad [\text{A13}]$$

$$n_{\pm}^x = \frac{1}{2}\begin{cases} \sigma_0(\sigma_0^2 + 1)\left(\cot^{-1}\sigma_0 - \frac{\sigma_0}{\sigma_0^2 + 1} \right), \\ \sigma_0(\sigma_0^2 - 1)\left(\frac{\sigma_0}{\sigma_0^2 - 1} - \coth^{-1}\sigma_0 \right), \end{cases} \qquad [\text{A14}]$$

$$n_{\pm}^z = \begin{cases} \sigma_0(\sigma_0^2 + 1)\left(\frac{1}{\sigma_0} - \cot^{-1}\sigma_0 \right), \\ \sigma_0(\sigma_0^2 - 1)\left(\coth^{-1}\sigma_0 - \frac{1}{\sigma_0} \right). \end{cases} \qquad [\text{A15}]$$

The demagnetizing factors for a spheroid satisfy the identity $2n_{\pm}^x + n_{\pm}^z = 1$. In particular, for a sphere $n_{\pm}^x = n_{\pm}^z = \frac{1}{3}$; in the cylindrical limit, $\sigma_0 \to 1$, $n_-^x = \frac{1}{2}$, $n_-^z = 0$; in the plate limit, $\sigma_0 \to 0$, $n_+^x = 0$, $n_+^z = 1$. The numerical tables of the demagnetizing factors for ellipsoids were first given in Refs. (23) and (24).

APPENDIX B

Generalized Hypergeometric Function

The generalized hypergeometric function $_1F_2(\alpha; \{\beta, \gamma\}; x)$ is given by the series (see, e.g., Ref. (22))

$$_1F_2(\alpha; \{\beta, \gamma\}; x) = \sum_{k=0}^{\infty} \frac{(\alpha)_k}{(\beta)_k(\gamma)_k} \frac{x^k}{k!}, \qquad [\text{B1}]$$

where $(\alpha)_k = \alpha(\alpha + 1)(\alpha + 2)\cdots(\alpha + k - 1)$.

The standard (Gaussian) hypergeometric function is

$$_2F_1(\{\alpha, \beta\}; \gamma; x) = \sum_{k=0}^{\infty} \frac{(\alpha)_k(\beta)_k}{(\gamma)_k} \frac{x^k}{k!}. \qquad [\text{B2}]$$

The asymptotic behavior of the function $_1F_2(-1/2; \{3/4, 5/4\}; -x^2/16)$, which appears in Eq. [50], is

$$_1F_2\left(-\frac{1}{2}; \left\{ \frac{3}{4}, \frac{5}{4} \right\}; -\frac{x^2}{16} \right) = \begin{cases} 1 + \frac{x^2}{30}, & x \ll 1, \\ \frac{|x|}{3}, & x \gg 1. \end{cases} \qquad [\text{B3}]$$

REFERENCES

1. A. Abragam, "Principles of Nuclear Magnetism," Oxford Univ. Press, New York (1989).

2. D. A. Yablonskiy, Quantitation of intrinsic magnetic susceptibility-related effects in a tissue matrix. Phantom study, *Magn. Reson. Med.* **39,** 417–428 (1998).

3. S. Ogawa, T. Lee, A. S. Nayak, and P. Glynn, Oxygenation-sensitive contrast in magnetic resonance image of rodent brain at high fields, *Magn. Reson. Med.* **14,** 68–78 (1990).

4. J. W. Belliveau, D. N. Kennedy, R. C. McKinstry, B. R. Buchbinder, R. M. Weisskoff, M. S. Cohen, J. M. Vevea, T. J. Brady, and B. R. Rosen, Functional mapping of the human visual cortex by magnetic resonance imaging, *Science* **254,** 716 (1991).

5. F. W. Wehrli, J. C. Ford, M. Attie, H. Y. Kressel, and F. S. Kaplan, Trabecular structure: Preliminary application of MR interferometry, *Radiology* **179,** 615–621 (1991).

6. S. Majumdar, D. Thomasson, A. Shimakawa, and H. K. Genant, Quantitation of the susceptibility difference between trabecular bone and bone marrow: experimental studies, *Magn. Reson. Med.* **22,** 111–127 (1991).

7. S. Ogawa, R. S. Menon, D. W. Tank, S.-G. Kim, H. Merkle, J. M. Ellerman, and K. Ugurbil, Functional brain mapping by blood oxygenation level-dependent contrast magnetic resonance imaging, *Biophys. J.* **64,** 803–812 (1993).

8. J. C. Ford, F. W. Wehrli, and H.-W. Chung, Magnetic field distribution in models of trabecular bone, *Magn. Reson. Med.* **30,** 373–379 (1993).

9. D. A. Yablonskiy and E. M. Haacke, Theory of NMR signal behavior in magnetically inhomogeneous tissues: The static dephasing regime, *Magn. Reson. Med.* **32,** 749–763 (1994).

10. R. M. Weisskopf, C. S. Zuo, J. L. Boxerman, and B. R. Rosen, Microscopic susceptibility variation and transverse relaxation: Theory and experiment, *Magn. Reson. Med.* **31,** 601-610 (1994).

11. R. P. Kennan, J. Zhong, and J. C. Gore, Intravascular susceptibility contrast mechanisms in tissues, *Mag. Reson. Med.* **31,** 9–21 (1994).

12. J. L. Boxerman, L. M. Hamberg, B. R. Rosen, and R. M. Weisskoff, MR contrast due to intravascular magnetic susceptibility perturbations, *Magn. Reson. Med.* **34,** 555–566 (1995).

13. L. A. Stables, R. P. Kennan, and J. C. Gore, Asymmetric spin-echo imaging of magnetically inhomogeneous systems: Theory, experiment, and numerical studies, *Mag. Reson. Med.* **40,** 432–442 (1998).

14. V. G. Kiselev and S. Posse, Analytical model of susceptibility-induced MR signal dephasing: Effect of diffusion in a microvascular network, *Magn. Reson. Med.* **41,** 499–509 (1999).

15. W. R. Bauer, W. Nadler, M. Bock, L. R. Schad, C. Wacker, A. Hartlep, and G. Ertl, The relationship between the BOLD-induced T(2) and T(2)(*): A theoretical approach for the vasculature of myocardium, *Magn. Reson. Med.* **42,** 1004–1010 (1999).

16. J. H. Jensen and R. Chandra, NMR relaxation in tissues with weak magnetic inhomogeneities, *Magn. Reson. Med.* **44,** 144–156. (2000).

17. D. A. Yablonskiy, G. L. Bretthorst, M. E. Raichle, and J. J. H. Ackerman, The structure of BOLD signal in functional MRI: Linear and nonlinear contributions, *in* International Society of Magnetic Resonance in Medicine, Seventh Scientific Meeting and Exhibition, Philadelphia, PA (1999).

18. S. C.-K. Chu, Y. Xu, J. A. Balschi, and C. S. Springer, Bulk magnetic susceptibility shift in NMR studies of compartmentalized samples: Use of paramegnetic reagents, *Magn. Reson. Med.* **13,** 239–262 (1990).

19. J. C. Maxwell, "Electricity and Magnetism," third ed., Clarendon Press, Oxford (1904).

20. L. D. Landau and E. M. Lifshitz, "Electrodynamics of Continuous Media," Pergamon Press, New York (1960).

21. D. A. Yablonskiy and E. M. Haacke, Theory of NMR signal dephasing in heterogeneous systems, *in* Society of Magnetic Resonance in Medicine, 12th Annual Meeting, New York (1993).

22. I. S. Gradstein and I. M. Ryzhik, "Table of Integrals, Series, and Products," fifth ed., Academic Press, New York (1999).

23. E. C. Stoner, Demagnetising factor for ellipsoids, *Phil. Mag.* **36,** 803–821 (1945).

24. J. A. Osborn, Demagnetising factor for the general ellipsoid, *Phys. Rev.* **67,** 351–356 (1945).